JOURNAL OF Applied Polymer SCIENCE

Carbon nanofibers from renewable bioresources (lignin) and a recycled commodity polymer [poly(ethylene terephthalate)]

Efstratios Svinterikos, Ioannis Zuburtikudis*

Department of Chemical and Petroleum Engineering, United Arab Emirates University (U.A.E.U), P.O. Box 15551, Al Ain, U.A.E

*Currently on a Leave of Absence from the Dept. of Mechanical and Industrial Design Engineering, TEI of Western Macedonia, Kozani, 50100, Greece

Correspondence to: I. Zuburtikudis (E-mail: ioannis.z@uaeu.ac.ae or izub@teikoz.gr)

ABSTRACT: Utilizing inexpensive biorenewable and waste raw materials for the production of carbon nanofibers can pave the way for lowering their manufacturing cost. In this research, lignin is combined with recycled poly(ethylene terephthalate) (PET) to fabricate precursor fibers via electrospinning. The process is optimized using the Design of Experiments statistical methodology and fibers with minimum average diameter equal to 191 ± 60 nm are prepared. Investigation with Attenuated Total Reflection – Fourier Transform Infrared Spectroscopy reveals the lignin structural changes induced by the solvent (trifluoroacetic acid), which is used for the preparation of homogeneous solutions of lignin and PET in various concentrations, while it gives an indication of the blending of the two electrospun polymers. The good miscibility between lignin and PET is also confirmed with Differential Scanning Calorimetry. The subsequent carbonization of the precursor fibrous mats results in a fibrous carbon structure with average fiber diameters similar to those of the precursor fibers. The successful transformation into carbon nanofibers is affirmed by Energy Dispersive X-ray Spectroscopy. The Carbon content of these nanofibers amounts to 94.3%. © 2016 Wiley Periodicals, Inc. J. Appl. Polym. Sci. **2016**, *133*, 43936.

KEYWORDS: biopolymers and renewable polymers; electrospinning; fibers; recycling; spectroscopy

Received 18 November 2015; accepted 16 May 2016
DOI: 10.1002/app.43936

INTRODUCTION

Carbon fibers have attracted the interest of research because of their unique properties including high tensile strength and stiffness, low density, high electrical conductivity, and good flexibility.[1–4] When their diameter is reduced to the submicron range, their surface area is maximized and they are termed as carbon nanofibers (CNFs). The strict use of the term "nanofibers" (either carbon or polymer nanofibers) demands that the fiber diameter does not exceed 100 nm. However, this term is very often used for fibers whose diameters are in the range of 100–500 nm in the relevant literature. An assembly of graphene sheets constitutes the internal structure of CNFs,[5a] having typically a carbon content of at least 92 wt %.[2] They have an array of applications in different technologies and industries such as in the automotive and aerospace industries, in sports equipment, in filtration technology, energy storage, catalysis, and electromagnetic shielding among others.[1–4,6,7]

Currently, the main route of commercial carbon fiber production is the thermal treatment of fibrous polymer precursors.[3,8] Their most common precursor is poly(acrylonitrile) (PAN), while pitch is secondarily used.[3,8] However, the high cost of PAN hampers the widespread use of CNFs, since the precursor cost accounts for up to 50% of their manufacturing cost.[8] In the recent years, research has focused on reducing the manufacturing cost by utilizing alternative raw materials, especially natural polymers such as lignin that come from biorenewable resources.

Lignin is the second most abundant natural polymer behind cellulose and the most important renewable source of aromatic structures on Earth.[9,10] It is a low-cost raw material obtained as a major by-product of paper industry.[9,11] Its structure is formed by radical polymerization of phenylpropane units (guaiacyl, syringyl and p-hydroxyphenyl propane units),[12] although its configuration varies among plant species.[10,12] The lignin macromolecules contain various functional groups, such as hydroxyl, carboxyl and carbonyl groups (Figure 1).[10]

Despite its utilization in several applications, there are no value-added products derived from lignin on a large scale.[2] There has been, however, a growing interest in its use as precursor for carbon

This article was published online on 6 June 2016. An error was subsequently identified in the author line and title page footnote. This notice is included in the online and print versions to indicate that both have been corrected 15 June 2016.

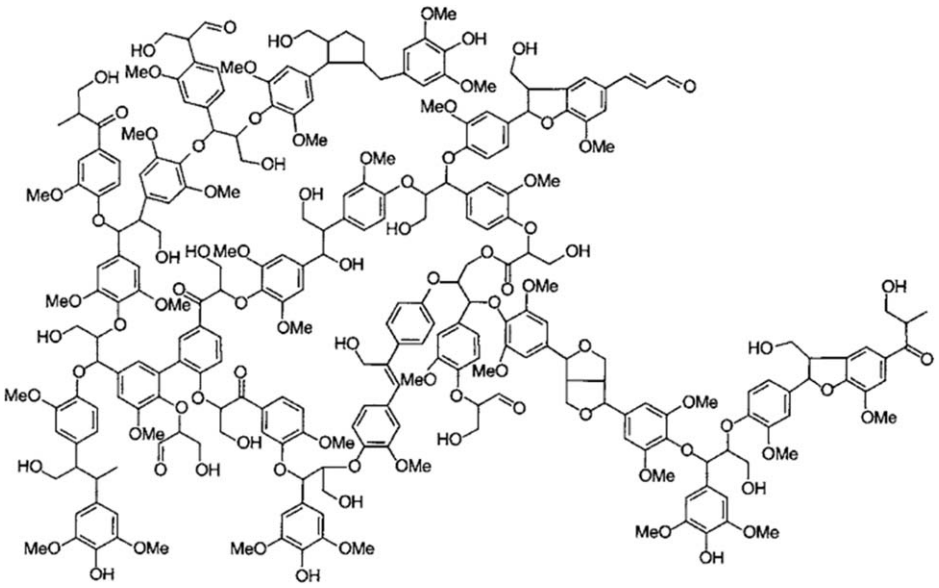

Figure 1. Proposed structure of beech lignin.[12]

fibers because of its relatively high carbon content (>60%), the absence of toxic by-products during carbonization, its availability and its low cost.[2] Either melt-spun or electro-spun, lignin has been successfully used as a precursor for carbon fibers either alone or blended with other polymers including poly(ethylene) (PE), poly (propylene) (PP), poly(ethylene terephthalate) (PET), poly(ethylene oxide) (PEO), poly(acrylonitrile) (PAN) and poly(vinyl alcohol) (PVA).[2–4,8,11,13–16] On the other hand, the total global consumption of plastics increases annually by 5–6%, while PET is the most recyclable plastic material.[17] It would be therefore desirable to develop alternative usages of recycled PET.

The motivation for the research presented here is to combine an inexpensive, natural and renewable polymer (lignin) derived from bio-waste matter with a recycled commodity polymer (PET) for the production of low-cost CNFs. In this way, the values of an industrial by-product (lignin) and a waste material (used, recycled PET) are significantly improved by manufacturing high added-value products, while environmental issues are addressed in a positive way.

According to published data concerning the cost of CNFs,[8] the production cost of conventional PAN carbon fibers ranges between \$12.25 and \$25.43 kg^{-1}, depending on the polymer grade and the process; a significant proportion of this price (up to 50%) is the cost of raw PAN. In addition, the production cost of lignin-based carbon fibers was estimated at around \$4–\$6.27 kg^{-1} depending on the yield[8]; this cost is significantly lower compared to PAN-based carbon fibers. Taking into consideration the low price of recycled PET (usually less than \$1 kg^{-1}), the production cost of CNFs from lignin/recycled PET is expected to be considerably reduced.

Blends of lignin with PET as carbon fiber precursors have been reported before.[4,18] Kadla *et al.*[4] reported the fabrication of kraft lignin/PET fibers with melt spinning. The ratio of PET varied between 0 and 25 wt %. Although this blend exhibited better spinnability than the blends of lignin with poly(ethylene) and poly(propylene), the fiber formation was more difficult compared to pure lignin, so the researchers didn't proceed with the carbonization process. Kubo and Kadla[18] further reported the melt spinning of kraft lignin blended with PET. The PET ratio varied between 0 and 100 wt % and the processing temperature between 195 °C and 273 °C. The produced carbon fibers' diameter ranged between 30 and 45 μm and improved tensile strength was reported compared to carbon fibers derived from pristine lignin. Because of good miscibility of the two materials the fiber surface was smooth, but the carbon fiber yield decreased with increasing the PET content. The researchers suggested that the good miscibility of the two materials probably derives from π-type interactions of the aromatic rings that both polymers contain in their molecules. The same researchers report elsewhere[19] that, in lignin/PET blends, there is no hydrogen bonding, but only weak intermolecular interactions. Finally, Compere *et al.*[20] also reported the fabrication of lignin/PET fibers by melt spinning and subsequent carbonization. The fiber diameters ranged between 11 and 13 μm.

Here, the precursor carbon fibers of lignin/recycled PET were fabricated with electrospinning, a well-established technique for the fabrication of micron- and nano-sized fibers. Briefly, the technique produces fibers by applying an electrostatic field between the tip of a syringe that contains the polymer solution and a grounded collector, which stretches the droplets of the polymer solution. The processing parameters (including the feed rate, the solvent, the polymer concentration, the spinning distance, the voltage and the temperature) can be controlled. Detailed information about the technique can be found elsewhere.[5b]

In the present article, we summarize the successful preparation of the electrospun lignin/PET precursor nanofibers following the Design of Experiments (DoE) statistical methodology and provide carbonization results that prove the creation of CNFs. In contrast to previous research, where the average diameter of the produced lignin/PET fibers was larger than 11 μm, we report the fabrication of precursor nanofibers with average diameter lower than 200 nm, which were transformed into CNFs of similar diameter.

Table I. Electrospinning Variables and Their Experimental Range

Variables	Experimental range
Flow rate (μL min^{-1})	0.1–2
Spinning distance (cm)	7–20
Voltage (kV)	20–30
Concentration of both polymers in the solution (% w v^{-1})	15–25
Lignin mass ratio in the polymer blend (wt %)	20–50

EXPERIMENTAL

Materials

Kraft lignin (alkali lignin, low sulfonate content, $M_w \sim 10{,}000$) was obtained from Sigma-Aldritch and was used as received. Since the idea behind this research was the combination of lignin with recycled PET for the fabrication of nanofibers, we did not use pristine PET, but already used PET water bottles. All the bottles that were used as the source for PET came from the same water-bottling company in the U.A.E. and were chosen for their availability (popular water brand). They were dried and cut into pieces for the preparation of the spinnable solutions.

The Melt Flow Index of the recycled PET was measured using a Chengde Jingmi (XRL-400) plastometer according to ASTM D1238. At 265 °C with 2.16 kg load the MFI was found 72 g 10 min^{-1}. This value is within the range found in the literature for PET which has undergone thermal processing cycles, such as extrusion or injection molding, as it is expected for PET scraps derived from water bottles.[21,22] An indicative MFI value for pristine PET found in the literature is 23 g 10 min^{-1}.[22,23]

Trifluoroacetic acid (TFA, 99%) purchased from Merck was used as solvent for the electrospinning, since TFA is commonly used as a solvent for the electrospinning of PET.[24–26] Solutions of lignin/PET with various concentrations (Electrospinning and Experimental Design section) were prepared and left under magnetic stirring at room temperature for 6 h until the PET pieces had been dissolved completely.

Electrospinning and Experimental Design

The electrospun mats were fabricated in a FUENCE E-sprayer (ES-2000S) apparatus in which the setup has vertical orientation. A 10 mL syringe (21G needle) was used. The grounded collector was moving horizontally during the process in a controlled pattern. The design variables of the electrospinning process were the flow rate of the solution, the distance between the needle and the collector (spinning distance), the applied voltage, the concentration of both polymers in the electrospinning solution and the lignin mass ratio in the polymer blend (Table I). The average fiber diameter was chosen as the measured response. The experiments were performed at room temperature (~23 °C) and the humidity was almost constant throughout the experiments (around 44–46%). Humidity was regarded as an uncontrollable factor, since it was not possible to adjust its level inside the chamber of the electrospinning apparatus; however it did not variate significantly.

In order to decide on the range of each electrospinning variable, some preliminary experiments were performed for finding out in which conditions the spinnability is acceptable. Because of the relatively low molecular weight of lignin ($M_w \sim 10{,}000$) and consequently the relatively low viscosity of the solutions, in some conditions there was spray (droplets) falling on the collector, especially at high flow rates, low voltage, low concentrations, and high lignin content. In addition, the electrospinning apparatus had restrictions regarding the values of the process variables that could be set; specifically, 20 cm spinning distance, 0.1 μL min^{-1} flow rate, and 30 kV voltage were the respective limits of the apparatus. The range of each variable was based on the demand of continuous fiber formation without spray. Regarding the range of the lignin mass ratio, when the lignin ratio was very high there was electrospray falling on the collector. On the other hand, we did not wish to use less than 20 wt % lignin, although there was successful fiber formation, because of our aim of using this biowaste material as carbon fiber precursor.

In order to minimize the response, an experimental design was employed. First, a 2^{5-1} resolution V fractional factorial design with 16 unreplicated randomized runs in two blocks and two center points in each block was constructed (20 experimental runs in total). The purpose of this screening factorial design was to examine the effects of the design variables on the response and identify which of them have the most significant influence. Subsequently, the method of steepest descent was implemented in order to find the optimum combination of the significant design variables. The experimental design was constructed and analyzed using the Minitab 17 software with 95% confidence interval. Extensive details on the experimental design, the statistical analysis of the results and the minimization procedure can be found elsewhere.[27]

Characterization

After the fabrication, all the electrospun samples were left to dry for 24 h at room temperature. The morphology of the fibrous mats was examined using Scanning Electron Microscopy (JEOL Neoscope JCM-5000). The necessary coating of the mats with a gold (Au) layer preceded their SEM examination. The mean fiber diameter was measured using an image analyzer (ImageJ, National Institutes of Health, U.S.A.). Around 100 measurements in each sample were used for the calculation of the mean diameter and the standard deviation. Measurements of the fiber diameters at several different spots of each SEM image were taken in order to ensure a representative average fiber diameter for each different sample (mat).

In addition, Attenuated Total Reflection-Fourier Transform Infrared Spectroscopy (ATR-FTIR) analysis was performed to investigate the possible structural alterations of lignin under the effect of trifluoroacetic acid, as well as the structure of the lignin/PET electrospun fibers. In the case of lignin, three different cases were examined: pristine, solvent-cast and electrospun (in reality "electrosprayed", see Electrospinning of Lignin section) lignin. In both solvent-cast and "electrosprayed" lignin, the concentration of lignin in TFA was 20% w v^{-1}. For the preparation of solvent-cast samples, pristine lignin was first dissolved in TFA and then,

the solution was cast onto petri dishes and left to dry for 72 h. The spectra were obtained using an IRPrestige-21/Shimadzu spectrophotometer with a MIRacle ATR tool by PIKE Technologies.

The miscibility between lignin and PET was examined through Differential Scanning Calorimetry (DSC) using a Netzsch DSC 200 F3 instrument. Five different compositions of the lignin/PET blend were investigated; namely 80/20, 65/35, 50/50, 35/65, and 20/80. Each blend was prepared by dissolving the appropriate quantities of polymers in TFA and then, following the electrospinning process they were spun into nanofibrous mats and left to dry for 72 h before monitoring their thermal behavior. For comparison, the thermogram of pristine untreated lignin as well as that of the starting recycled PET were also recorded. For each measurement, a sample of 9–10 mg was tested in the range 40–300 °C with a scan rate of 10 °C min^{-1}.

Carbonization

The electrospun mats were carbonized following relevant published protocols for lignin.[4,11] First, the precursor fibers were thermo-stabilized in air with a heating rate of 120 °C h^{-1} until they reached 260 °C, where they were held for 1 h. Then, the carbonization took place in N_2 atmosphere; the heating rate was 180 °C h^{-1} until the temperature of 1000 °C was reached; the samples were held at 1000 °C for 1 h. A temperature-programmed tubular furnace (Tube Furnace GSL-1500X-50, MTI) was used for these carbonization experiments.

The morphology of the carbonized mats was investigated via Scanning Electron Microscopy using either a JEOL 6610LV or a JEOL 6390A microscope after gold coating them (Q150R S, Quorum). The elemental composition of the these carbonized mats was examined with Energy Dispersive X-ray Spectroscopy (EDS) (X-MAX 80, Oxford Instruments) and analyzed using the AZtech Nanoanalysis software (Oxford Instruments).

RESULTS AND DISCUSSION

Electrospinning of Lignin

The choice of trifluoroacetic acid as a solvent was made because of its suitability for the electrospinning of PET.[24–26] PET is insoluble in the common solvents used in the literature for the electrospinning of lignin (H_2O, N,N-dimethylformamide, acetonitrile, ethanol, etc.).[9,11,13,16,28–30] However, the behavior of lignin in TFA is rather ambiguous. TFA has been proposed as a solvent for the treatment and fractionation of plant biomass in order to separate and recover various useful components (cellulose, lignin, non-cellulosic polysaccharides).[31,32] In this context, Morrison and Steward[31] reported that most of the lignin of oat straw is insoluble to TFA, with Poirier *et al.*[33] presenting similar results for lignin derived from maize leaves and attributing this feature to some degree of cross-linking. In addition, Fanta *et al.*[34] stated that ~10% of lignin derived from wheat straw underwent degradation in TFA and gave water soluble fractions. Similar results were reported by Dong *et al.*[32] Other researchers who used TFA for the electrospinning of lignocellulosic fibers[35,36] report that the dissolution of lignin in TFA includes the cleavage of some covalent bonds and the disruption of the 3D network. Moreover, the hydroxyl groups of lignin create ester bonds with TFA, a process which, however, is reversible in atmospheric conditions.[35,36] In our experiments, kraft lignin was found totally soluble in TFA. In general, the chemical properties of lignin depend on its plant source, the extraction process and possible post-treatment. Probably some of these variables defined this behavior in our case. However, some degree of degradation was expected. The possible structural modification of lignin dissolved in TFA was studied with ATR-FTIR (Structural investigation with ATR-FTIR section).

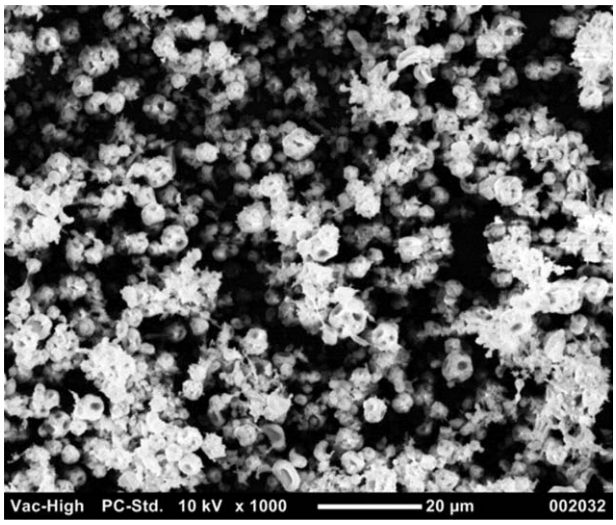

Figure 2. SEM image of electrospun (electrosprayed) lignin 30% w v^{-1} in TFA.

The attempts to produce fibers of pure lignin were unsuccessful. Instead of electrospun fibrous mats, there was just electrospray (Figure 2). This has been observed previously with solutions of kraft lignin in water or N,N-dimethylformamide.[11,13,28–30] This behavior is attributed to the relatively low molecular weight of kraft lignin resulting in the absence of extensive chain structures and/or molecular entanglements.[30] Therefore, the presence of PET as a binder polymer is determinant for successful electrospinning. Dallmeyer *et al.*[29] reported that the electrospinnability of lignin in the presence of a binder polymer [in their case poly (ethylene oxide)] is dependent on the viscoelastic properties of the solution, as an increase in shear modulus and strain hardening was observed. The interaction between lignin and PET is obviously important for the successful fiber formation. The nature of this interaction was studied by Kadla and Kubo.[19] Although both polymers possess functional groups capable of forming hydrogen bonds, they concluded that only a minor degree of such interaction existed between the two polymers. Instead, the fact that the glass transition temperature of the blend (T_g) exhibited negative deviation from a linear mixing rule was an indication of weak specific intermolecular interactions.

Electrospinning of Lignin/PET Blend

The Significant Variables. Figure 3 presents some SEM images of characteristic mat morphologies fabricated at various electrospinning conditions. The results showed that the average fiber

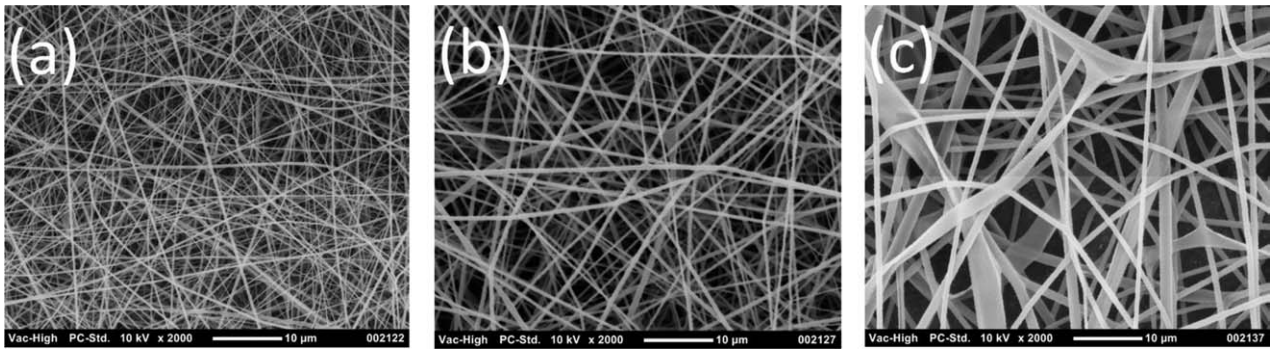

Figure 3. Examples of mat morphologies with varying fiber diameters; (a) 278 ± 88 nm, (b) 508 ± 168 nm, (c) 1144 ± 560 nm. Scale bar is 10 µm in all images.

diameter ranged vastly from 229 ± 84 nm to 1473 ± 575 nm for different sets of conditions.

The analysis of variance performed for the screening factorial design revealed those electrospinning variables, which have the most significant effect on the response. These were the solution concentration and the spinning distance. The other three variables were found to have no significant effect on the average fiber diameter for the chosen range of values. A probable explanation of this behavior lies on the relatively narrow experimental range of these variables. However, this range was defined by the demand of acceptable spinnability and was also restricted by the apparatus' allowable limits in voltage and distance between the tip and the collector. Even so, all of the variables influence the response through their two- or three-way interactions. The magnitude of the effects on the response is presented in the normal plot of Figure 4.

Here, points that fall far from the line indicate significant effects, and their magnitude is proportional to their distance from the line. The statistical analysis of the design gave the values of 99.24% for R^2, 85.46% for R^2 (prediction) and 0.000 for the P value of the model; thus, there is a strong indication that the model adequately describes the data.

Minimization of the Fiber Diameter. The surface plot of the average fiber diameter as a function of the two significant variables (concentration and distance) is presented in Figure 5. The two marked areas signify the experimental regions in which the average fiber diameter is minimized.

As can be seen from the surface plot of Figure 5, in order to minimize the diameter, low values of concentration are needed. This behavior is well-described in the literature.[5b,6,26,29,30,37] Solutions with lower concentration have lower viscosity; so, as the jet travels towards the collector, the low viscosity promotes the extension of the jet, resulting in thinner fibers.[6]

The effect of spinning distance is, however, more complicated and different behavior has been reported for different systems.[5b,34–43] Here it seems that the response is minimized either at very low or at very high values of distance. Probably this happens because of antagonistic effects, which are affected by the strength of the electric field (the ratio of voltage over distance). At small spinning distance and constant voltage, the electrostatic field is stronger; so, it exerts higher electrostatic forces on the jet and elongates the fibers. Simultaneously, the strong field causes higher mass flow tending to increase the fiber diameter.[43] At higher distances, these effects are reversed, but the fibers have more time to elongate; hence, this intricate relationship.

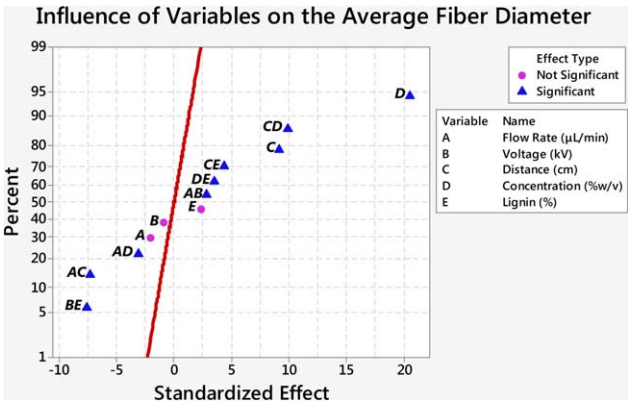

Figure 4. The influence of each electrospinning variable on the average fiber diameter. [Color figure can be viewed in the online issue, which is available at wileyonlinelibrary.com.]

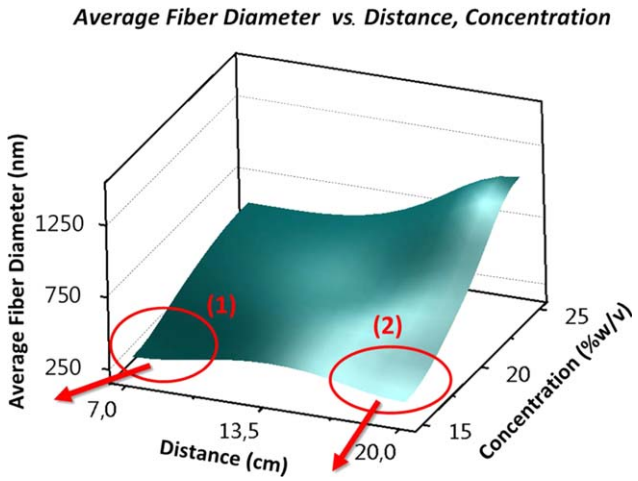

Figure 5. Surface plot of the average fiber diameter as a function of spinning distance and solution concentration. [Color figure can be viewed in the online issue, which is available at wileyonlinelibrary.com.]

The surface plot of Figure 5 reveals that the steps for diameter minimization should focus on two distinct areas: (1) lower concentration combined with the lowest distance or (2) lower concentration combined with the highest distance. The shape of the surface plot in these two areas indicates that probably the point of minimization lies beyond the experimental area initially explored. This is what the two arrows demonstrate. So, in order to find the conditions in which the diameter is minimized, the plot borders should be expanded and the areas beyond should be explored. However, the distance of 20 cm was the maximum allowed by our electrospinning apparatus, so, in area (2), only the effect caused by minimizing the concentration could be investigated. Following the method of Steepest Descent,[44] we explored the paths for the minimization of the average fiber diameter, moving towards the direction shown by the two arrows. Four additional experimental points beyond the plot borders were examined in area (1) and five points in area (2). The step and direction of proceeding in these two experimental regions, as well as detailed results are described more extensively elsewhere.[27]

The behavior of the system was similar in both areas. Moving along the experimental paths indicated by the arrows in Figure 5, the mean fiber diameter decreased gradually, but at the same time there was a progressive appearance of beads until they totally prevailed. This behavior is expected and is explained by the effect of concentration; very low concentration means very low viscosity, so the jet breaks into droplets and beads are formed on the collector. The fibers in area (1) had lower diameter and narrower distribution than those in area (2). Because beads are not acceptable, we decided to regard the experimental point of minimum beads as the desirable combination of variables. The point of minimum average diameter appeared in area (1). At this point, the measured value of average diameter is 191 ± 60 nm; this value and the relative range were confirmed by replicating the electrospinning process under the same conditions. The corresponding optimum combination of electrospinning variables is: Concentration = 10% w v^{-1}, Distance = 7.7 cm, Voltage = 30 kV, Lignin ratio = 50 wt %, and Flow rate = 0.1 μL min^{-1}.

Structural Investigation with ATR-FTIR

Lignin. In order to assess the possible influence of TFA in the structure of lignin, the ATR-FTIR spectra of pristine, solvent-cast, and electrospun (electrosprayed) lignin were examined and are shown in Figure 6.

This figure presents the absorption bands (a) in the region 4000–500 cm^{-1} and (b) in the magnified region 1900–500 cm^{-1}. The spectra contain the typical peaks found in the literature for lignin samples.[45–49] Table II summarizes the peaks detected in the pristine lignin sample and their assigned types of vibration. The solvent-cast and the electrospun (electrosprayed) lignin samples exhibited differences in their spectra compared to pristine lignin. Because of the similarity between the spectra of solvent-cast and electrosprayed lignin, in Figure 6 only the peaks of the latter are marked.

The most important differences between the spectrum of the electrospun (electrosprayed) lignin and that of the pristine lignin are:

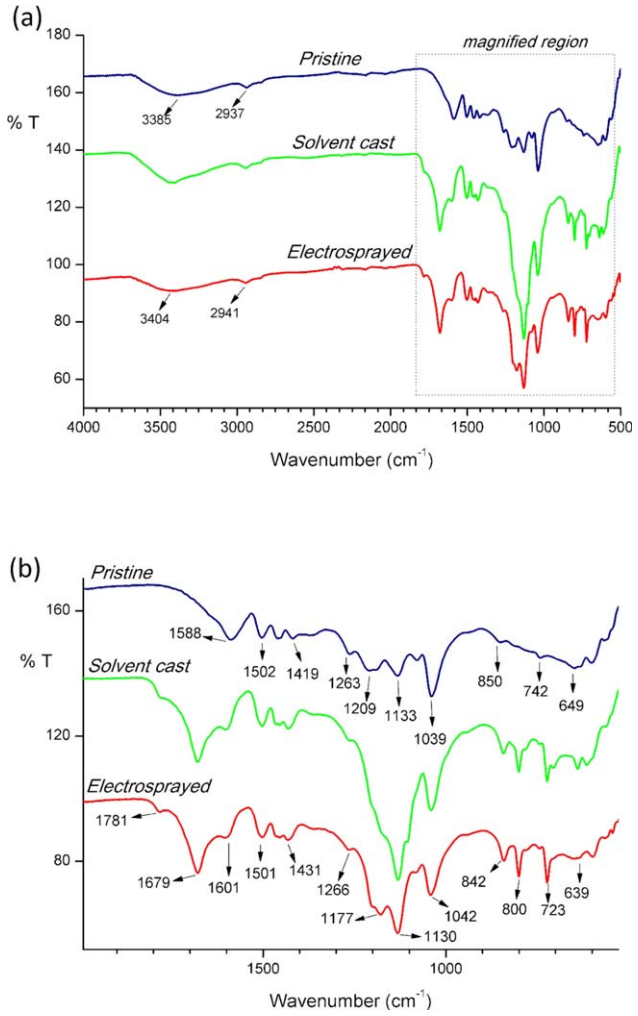

Figure 6. ATR-FTIR spectra of the lignin samples, (a) wavenumber from 4000 to 500 cm^{-1} and (b) magnified region of IR spectra (1900–500 cm^{-1}). [Color figure can be viewed in the online issue, which is available at wileyonlinelibrary.com.]

- Solvent-cast and electrosprayed lignin exhibit a large absorption band in the area 1650–1800 cm^{-1}. This band probably corresponds to vibrations of C═O groups either in conjunction or not with the aromatic ring,[45–49] probably associated with guaiacyl units.[47] The appearance of these bands could be an indication of cleavage of ester linkages.[47] The peak in the region of 1781 cm^{-1} may signify the presence of trifluoroacetyl groups, since TFA can act as esterifying agent of hydroxyl groups present in lignin.[35,36]
- The most significant difference between pristine and electrosprayed lignin is the huge increase in absorption in the area 1100–1200 cm^{-1}. This area is associated with deformation vibrations of C—H bonds in the aromatic rings[16,45,47] probably in syringyl units[45,47] and is also associated with some possible overlapping of stretching vibrations of C—O bonds.[45,46] This could signify a higher number of un-substituted positions in the aromatic ring or rearrangement of peripheral groups attached to it.[51] The mechanism of this effect, induced by the strong acid, is not clear. Similar observations are found elsewhere.[48,51,52] In Ref.

Table II. Absorption Peaks and Types of Vibrations in the Pristine Lignin Sample

Peak location (cm^{-1})	Type of vibration
3385	Stretching vibrations of alcoholic and phenolic —OH groups involved in hydrogen bonds[45]
2937	CH stretching (—CH_3 or —CH_2—)[47,48]
1588	Aromatic ring vibrations[45]
1502	Aromatic ring vibrations[45]
1458	Aromatic ring vibrations/asymmetric deformation of C—H stretching[48,49]
1419	Aromatic ring skeletal vibrations combined with C—H in-plane deformation[16,45,47]
1263	Vibrations of guaiacyl rings and stretching vibrations of C—O bonds[45,47]
1209	Vibrations of guaiacyl rings and stretching vibrations of C—O bonds[45,50]
1133	Deformation vibrations of C—H bonds in the aromatic rings - syringyl units[16,45,47]
1039	Vibrations of C—H bonds in guaiacyl rings/C—O stretching in O-CH_3, C-OH groups[45-49]
850	Deformation vibrations of C—H bonds associated to guaiacyl[45,48]
742	Deformation vibrations of C—H bonds associated to aromatic rings[45]
649	Out-of-plane -OH bend[49]

52 some possible mechanisms of rearrangement in the lignin structure are speculated. In this area, there is also the only significant difference between solvent-cast and electrosprayed lignin, possibly because of the stretching effect of electrostatic field.

- Solvent-cast and electrosprayed lignin have intense absorption peaks in the region 640–850 cm^{-1}. These peaks are attributed to deformation vibrations of C—H bonds in aromatic rings[45] or C—H out-of-plane vibrations in guaiacyl units[48]; perhaps another indication of un-substituted positions in the aromatic ring or rearrangement of peripheral groups.
- Generally in most peaks there is a shift towards higher or lower wavenumber values between pristine and electrosprayed lignin, indicating small structural differences between them.

Lignin/PET Blend. Figure 7 unveils the ATR-FTIR spectrum of electrospun lignin/PET mats in comparison with the spectra of electrospun (electrosprayed) lignin and of the raw recycled PET that was used in the experiments. The electrospun PET had identical spectrum with the raw PET, so we chose to present only the former. The electrospun lignin/PET mat, whose spectrum is presented here, consisted of a 50–50 lignin-PET blend. Spectra of different lignin-PET ratios exhibited absorption peaks at the same wavenumbers. Table III summarizes the absorption peaks of electrospun PET and their respective types of vibrations as described in the literature. In our case, the most distinctive peaks of the PET spectrum appear in 1719, 1408, 1242, 1095, 1018, 872, and 723 cm^{-1}. These peaks appear in the electrospun lignin/PET mat almost at the same wavenumbers. The same happens with the main lignin absorption peaks (see Table III). The fact that most of the peaks in the blend appear unchanged compared to those of the pure polymers, is an indication of weak intermolecular interactions between them.

Kadla and Kubo[19] reported that in the blend of lignin with PET, the intermolecular bonds consisted mainly of weak intermolecular interactions rather than hydrogen bonding. In our case, in the area around 3300–3500 cm^{-1}, which corresponds to hydroxyl stretching because of hydrogen bonding, there is a shift in the peak (from 3418 to 3447 cm^{-1}). This is a possible indication of some degree of hydrogen bonding development between the two polymers. However, the peak at 1719 cm^{-1}, which shows the C=O stretching in the PET molecules, appears almost unchanged in the blend; therefore, we can assume that there is only a small degree of hydrogen bonding, in accordance with the observations by Kadla and Kudo.

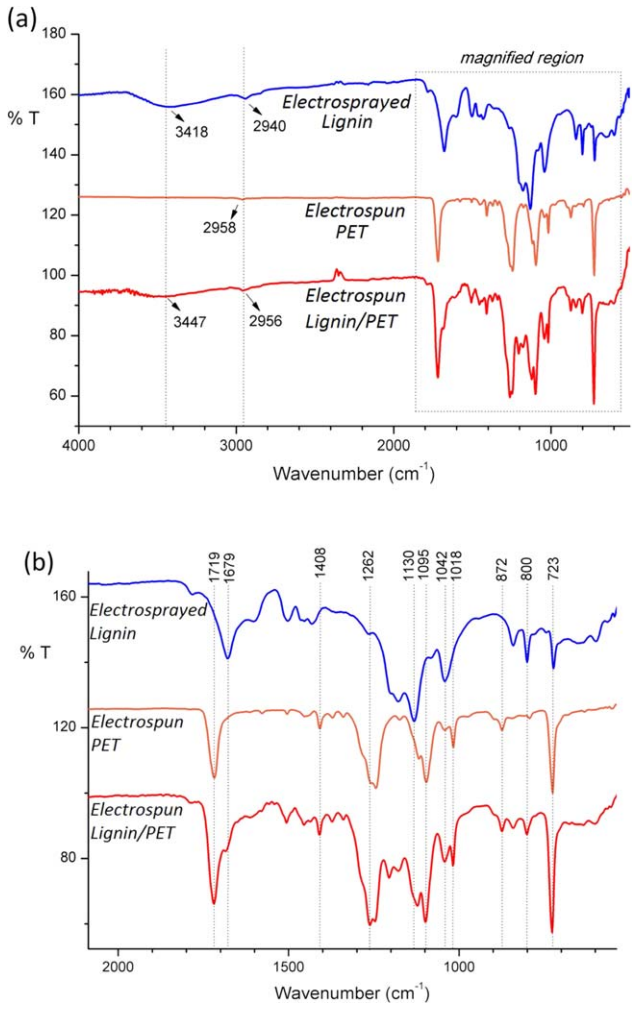

Figure 7. ATR-FTIR spectrum of electrospun lignin/PET mat in comparison with the spectra of electrospun (electrosprayed) lignin and electrospun PET, with (a) presenting the whole region (wavenumber from 4000 to 500 cm^{-1}) and (b) presenting the magnified region (2100–600 cm^{-1}). [Color figure can be viewed in the online issue, which is available at wileyonlinelibrary.com.]

Table III. Absorption Peaks and Types of Vibrations in the Electrospun PET Sample

Peak location (cm^{-1})	Type of vibration
1719	C=O stretching[50]
1408	Para-substituted benzene ring, ring C—H in-plane deformation, ring C-C stretching[50]
1242	(C=O)—C stretching of ester, ring-ester in-plane mode, amorphous phase[50,53]
1095	Ester C=O stretching/O-CH_2 stretching, in-plane ring mode, amorphous phase[50,53]
1042	Gauche O-CH_2 stretching, amorphous phase, gauche conformation[50]
1018	Para-substituted benzene ring, ring C—H in-plane deformation, gauche conformation[50,53]
872	Para-substituted benzene ring, ring C—H out-of-plane vibration, crystalline phase[50,53]
723	Ring C—C bending and ring C—H out-of-plane[50,53]

Thermal Behavior and Miscibility of the Lignin/PET Blend

A common way of assessing the miscibility of polymers is by monitoring the thermal behavior of their blends in various compositions. The appearance in the blends of a single glass transition temperature (T_g), which is dependent on the blend composition, signifies full miscibility at a dimensional scale between 5 and 15 nm.[19] The appearance of two distinct glass transition temperatures, however, is an indication of immiscible polymers.

Figure 8 presents the DSC curves of the electrospun mats prepared from lignin/PET blends of various compositions. In addition, the thermograms of the pristine untreated lignin (100/0) and the starting recycled PET (0/100) are presented. In order to reveal more details about the thermal behavior of PET, its thermogram in the region 60–130 °C is magnified. The recycled PET has T_g at 70.5 °C as indicated by the respective slope appearing at that region. The large endothermic peak at 250.9 indicates its melting temperature (T_m), while the broad exothermic plateau in the region 95–120 °C is associated with its cold crystallization temperature (T_{cc}). The T_{cc} of pure PET generally appears in the region between 100 °C and 160 °C, while its T_g is generally between 70 °C and 80 °C.[21–23,54] On the other hand, the T_g of lignin generally varies depending on its source, while it does not exhibit any melting temperature since it is amorphous because of its complex structure.[55–57] Here, the T_g of lignin appears at approximately 88.7 °C. One can observe that each lignin/PET blend has one single T_g which depends on the blend composition. Increasing the mass fraction of lignin, there is a slight gradual increase in the T_g of the blend from the curve of pure PET (0/100) towards the curve of pristine lignin (100/0). It can be deduced that the incorporated amorphous lignin interacts with PET at molecular level and restricts the motion of the polyester macromolecules, raising its T_g. Therefore, there is evidence that the two polymers are miscible.

Because of the close proximity of the glass transition temperature between pristine lignin and raw PET, as well as the moderate inclination that the DSC curves exhibit at that region, there could be a possibility of overlapping between two separate peaks; this scenario would conceal the possible immiscibility between lignin and PET. Nevertheless, this case should be rejected since the T_{cc} and T_m peaks provide a collateral evidence for the good miscibility of the two polymers. It is clear that the cold crystallization region in the raw PET shifts gradually towards higher temperatures with increasing lignin content, until it disappears for lignin mass fraction higher than 65 wt % (the trend is highlighted with the dashed ellipses in Figure 8).

In addition, the melting temperature of PET gradually decreases with increasing lignin content (from 250.9 °C at 0 wt % lignin to 242.3 °C at 35 wt % lignin) until it practically vanishes for more than 50 wt % lignin content. This is an indication of amorphous structure, or perhaps only minor regions in the blend are crystalline, which are undetectable in the thermograms. It can be inferred from the observations regarding T_g, T_{cc}, and T_m, that lignin interacts with the polyester macromolecules, restricts their mobility and impedes their crystallization.

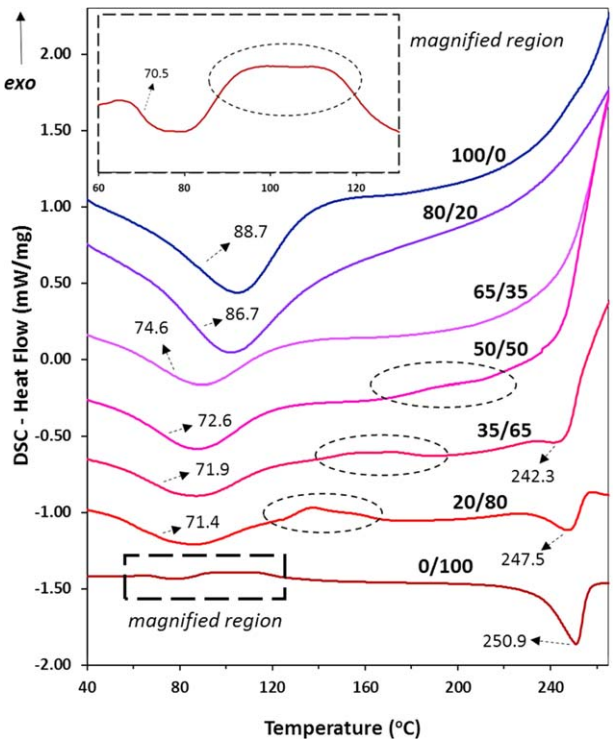

Figure 8. DSC thermograms of: electrospun mats prepared from various lignin/recycled PET blends (80/20, 65/35, 50/50, 35/65, 20/80), the pristine untreated lignin (100/0) and the starting recycled PET (0/100). The dashed ellipses indicate the regions of cold crystallization. The magnified region shows more clearly the DSC curve of PET in the region 60–130 °C. [Color figure can be viewed in the online issue, which is available at wileyonlinelibrary.com.]

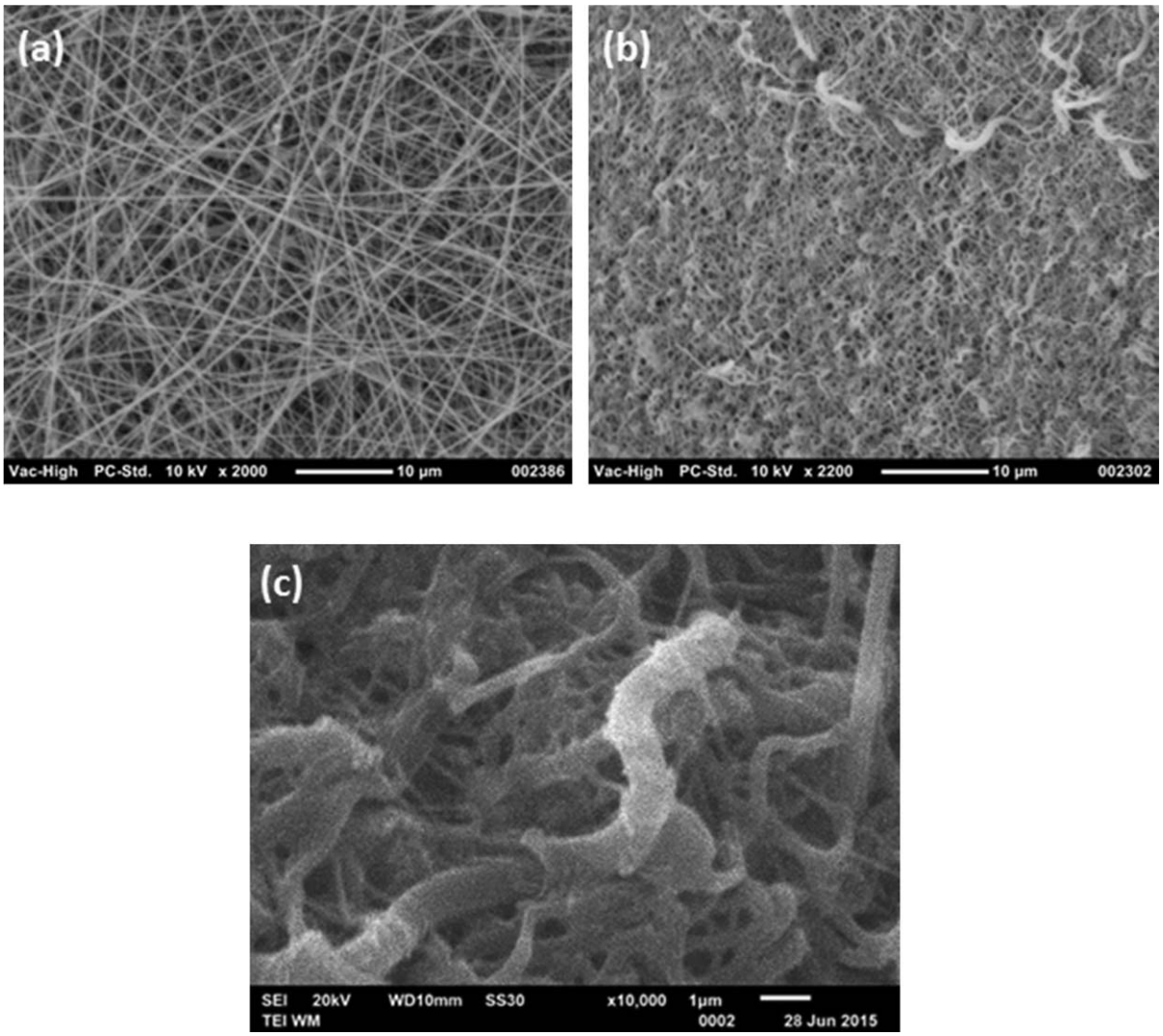

Figure 9. Lignin/PET precursor fibers of 280 ± 46 nm average diameter, (a) before and (b,c) after carbonization. Scale bar in (a) and (b) is 10 µm, while in (c) it is 1 µm.

The lignin–PET interactions disrupt the integrity and purity of PET spherulites and induce a drop in the melting temperature of the polyester. Similar behavior has been reported for the blend of lignin with poly(lactic acid).[57,58] These results provide therefore strong support to the hypothesis that lignin and PET exhibit good miscibility, and agree with previous observations for the same polymers.[19]

Carbonization Results

The carbonization process involves two steps in general: Oxidative thermo-stabilization at temperatures of 200–300 °C followed by carbonization under an inert atmosphere at temperatures higher than 600 °C. In the present research, we followed a carbonization protocol similar to those described in the literature for lignin samples[4,11] (Carbonization section).

The carbonization of precursor polymer fibers does not necessarily lead to carbon fibers, since not all polymers remain thermally stable and infusible during the thermostabilization and carbonization process (e.g., polyethylene, polystyrene).[2] The precursor fiber diameter also affects the structure after carbonization, since deformation and shrinkage are usual phenomena, especially in the case of lignin.[7] The precursor lignin/PET fibers reported in the literature so far, presented diameters larger than 10 µm and exhibited some degree of deformation and shrinkage during carbonization. Therefore for precursor fibers with diameters of around 200 nm, as in the present research, the contingency of yielding a completely shapeless structure after carbonization instead of carbon fibers could not be excluded.

Carbonization results of the lignin/PET fibers are presented in Figures 9–11. Here, the results for the successful carbonization of three samples with different average fiber diameters are presented, as an example which confirms the feasibility of the concept. Similar results were taken after carbonizing the other fibrous precursor mats, as well. The samples presented in Figures 9 and 10 were chosen from the ones fabricated during the initial factorial experimental design, which were subsequently carbonized. The mat shown in Figure 11 was fabricated under the same electrospinning conditions, which resulted in the minimum average diameter (see Minimization of the fiber diameter section). All three samples shown here were produced form

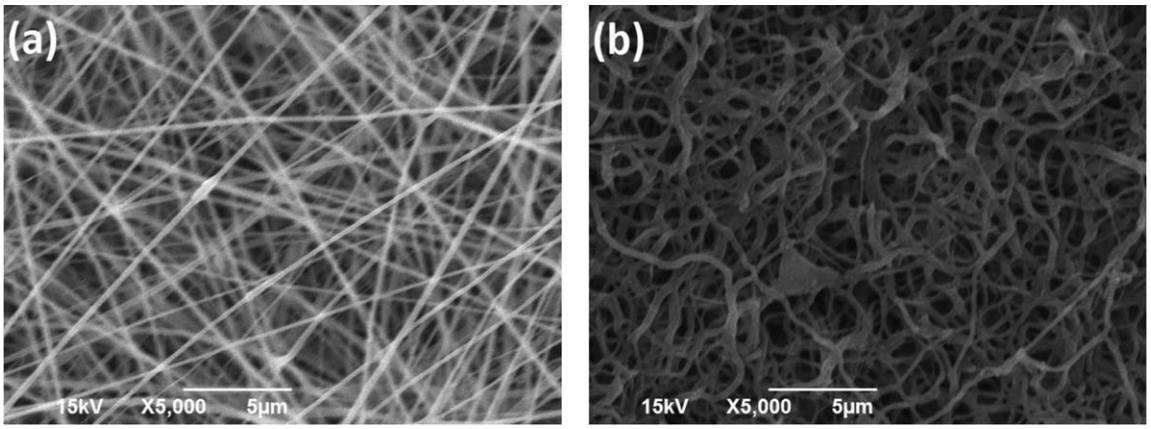

Figure 10. Lignin/PET precursor fibers of 241 ± 70 nm average diameter, (a) before and (b) after carbonization. Scale bar is 5 μm in both images.

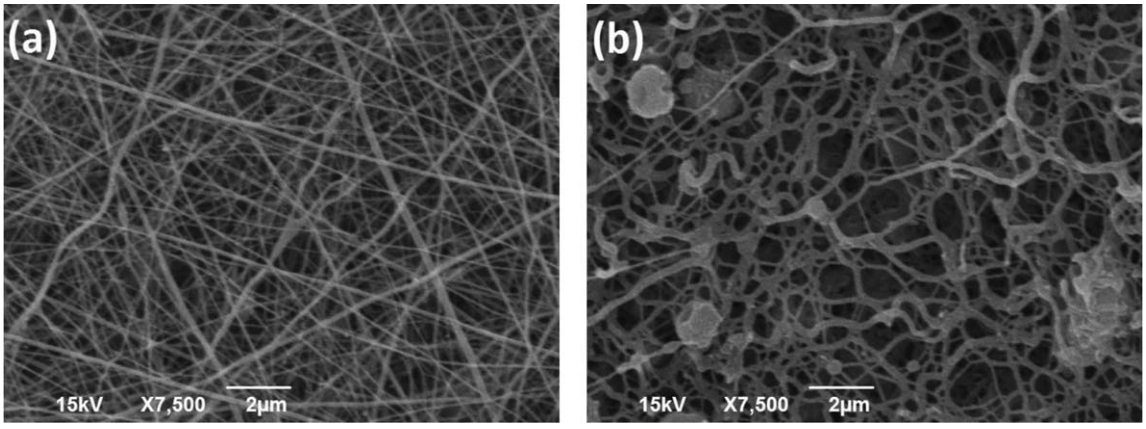

Figure 11. Lignin/PET precursor fibers of 163 ± 35 nm average diameter, (a) before and (b) after carbonization. Scale bar is 2 μm in both images.

precursor fibers of a 50/50 lignin/PET blend, under various electrospinning conditions corresponding to specific runs of the factorial design. In our ongoing research we are focusing on the carbon structure itself and the carbonization process, investigating the effect of several factors on the carbon morphology, including the lignin/PET ratio.

Figure 9 shows the morphology of a lignin/PET sample, with average precursor fiber diameter of 280 ± 46 nm, before (a) and after (b,c) carbonization. Careful examination with SEM confirms the creation of fibrous carbon morphology; the diameter measurements in the carbonized sample shown here gave the value of 290 ± 43 nm, which reveals that the fiber diameter was kept at the same levels as in the precursor fibers. Similarly, the precursor fibrous mat in Figure 10(a) has an average diameter of 241 ± 70 nm, while the corresponding carbonized mat exhibits an average diameter of 237 ± 72 nm [Figure 10(b)].

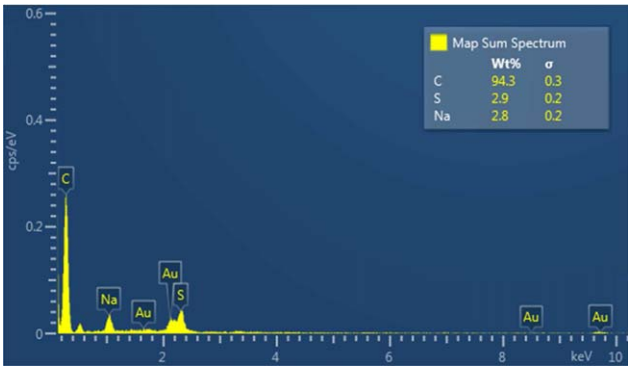

Figure 12. EDS Spectrum of the carbonized sample. [Color figure can be viewed in the online issue, which is available at wileyonlinelibrary.com.]

Figure 11 presents the carbonization results of the precursor fibers fabricated under the conditions which give the minimum diameter (see Minimization of the fiber diameter section). It was mentioned in Minimization of the fiber diameter section that under these conditions, precursor fibers of 191 ± 60 nm were produced. Replication of the electrospinning process under these conditions produced a mat with average diameter of 163 ± 35 nm [Figure 11(a)], which is within the range of diameters expected (191 ± 60). The corresponding carbonized fibrous mat has an average diameter of 155 ± 42 nm [Figure 11(b)], similar to the precursor fibers.

There is definitely fiber deformation, fusion, and interfiber bonding in all samples, which has been described again in the literature for lignin[7] and was possibly promoted by the presence of PET. It seems that the phenomenon is more intense as the fiber diameter

decreases. This could probably be controlled by adjusting the heating rate, the ratio of lignin or other parameters and is one of the objectives in the immediate-future optimization of the carbonization process, although in some applications such as energy storage devices, fusion could be desirable.[8] The EDS spectrum of the carbonized sample of Figure 9, which is shown in Figure 12, confirmed the transformation of the precursor fibers into CNFs with a C content amounting to 94.3%. The detection of Na and S can be attributed to the possible presence of ash in the kraft lignin.[46] Traces of Au because of the gold-coating of the SEM samples are also present in the EDS spectrum.

CONCLUSIONS

A method of combining an abundant natural raw material such as lignin with low-cost recycled PET for producing CNFs has been demonstrated. Through a well-established nanomanufacturing process, the electrospinning, precursor nanofibers were produced. Following the DoE statistical methodology, it was identified that the most significant variables for minimizing the average diameter were the solution concentration and the spinning distance for the range of values examined. By optimizing the process, the average diameter of precursor nanofibers was reduced to the value of 191 ± 60 nm. Examination of the electrospun mats with ATR-FTIR revealed the structural changes of lignin under the effect of TFA and provided an indication for the blending of the two polymers via weak intermolecular interactions. Evidence of the good miscibility between lignin and PET was also provided by DSC measurements. The transformation into carbon nanofibrous structure after thermostabilization and carbonization of the precursors was confirmed with EDS. The average diameter of the CNFs was retained at the same levels as those of the precursor fibers and their C content amounted to 94.3%. Minimization of the diameter at such levels results in maximization of the surface area, enhancing their capability as reinforcing material in automotive, military, aerospace or construction applications and providing a promising solution for numerous other uses in which the nano-sized dimension is significant, such as in the separation technology or energy storage devices. Future work will focus on the optimization of the carbonization process and the thorough characterization of the CNFs in conjunction with our intended applications, which lie in the field of advanced separations.

ACKNOWLEDGMENTS

The authors would like to thank Apostolos Baklavaridis, MSc Material Scientist and collaborator of the NanoMaMa Lab (www.nanohybrid.eu), for taking the SEM image (c) of Figure 9 and the EDS spectrum of Figure 12 using the SEM facilities of T.E.I. of Western Macedonia in Greece, the mother institute of Ioannis Zuburtikudis.

REFERENCES

1. Xu, X.; Zhou, J.; Jiang, L.; Lubineau, G.; Payne, S. A.; Gutschmidt, D. *Carbon* **2014**, *80*, 91.
2. Frank, E.; Steudle, L. M.; Ingildeev, D.; Spörl, J. M.; Buchmeiser, M. R. *Angew. Chem. Int. Ed* **2014**, *53*, 5262.
3. Frank, E.; Hermanutz, F.; Buchmeiser, M. R. *Macromol. Mater. Eng.* **2012**, *297*, 493.
4. Kadla, J. F.; Kubo, S.; Gilbert, R. D.; Venditti, R. A. In Chemical Modification, Properties, and Usage of Lignin; Hu, T. Q., Ed.; Kluwer Academic/Plenum Publishers: New York, **2002**; p 121.
5. Ko, F.; Wan, Y. Introduction to Nanofiber Materials; Cambridge University Press: Cambridge, **2014**; a) p 223, b) pp 49–58.
6. Gu, S. Y.; Ren, J.; Vancso, G. J. *Eur. Polym. J.* **2005**, *41*, 2559.
7. Dallmeyer, I.; Lin, L. T.; Li, Y.; Ko, F.; Kadla, J. F. *Macromol. Mater. Eng.* **2014**, *299*, 540.
8. Baker, D. A.; Rials, T. G. *J. Appl. Polym. Sci.* **2013**, *130*, 713.
9. Ruiz-Rosas, R.; Bedia, J.; Lallave, M.; Loscertales, I. G.; Barrero, A.; Rodríguez-Mirasol, J.; Cordero, T. *Carbon* **2010**, *48*, 696.
10. Duval, A.; Lawoko, M. *React. Funct. Polym.* **2014**, *85*, 78.
11. Jin, J.; Yu, B.; Shi, Z.; Wang, C.; Chong, C. *J. Power Sources* **2014**, *272*, 800.
12. Wool, R. P.; Sun, X. S. *Bio-Based Polym. Compos.* **2005**, 551.
13. Lai, C.; Zhou, Z.; Zhang, L.; Wang, X.; Zhou, Q.; Zhao, Y.; Wang, Y.; Wu, X. F.; Zhu, Z.; Fong, H. *J. Power Sources* **2014**, *247*, 134.
14. Xu, X.; Zhou, J.; Jiang, L.; Lubineau, G.; Chen, Y.; Wu, X. F.; Piere, R. *Mater. Lett.* **2013**, *109*, 175.
15. Lai, C.; Kolla, P.; Zhao, Y.; Fong, H.; Smirnova, A. L. *Electrochim. Acta* **2014**, *130*, 431.
16. Salas, C.; Ago, M.; Lucia, L. A.; Rojas, O. *J. React. Funct. Polym.* **2014**, *85*, 221.
17. Wang, C. Q.; Wang, H.; Liu, Y. N. *Waste Manag.* **2015**, *35*, 42.
18. Kubo, S.; Kadla, J. F. *J. Polym. Environ.* **2005**, *13*, 97.
19. Kadla, J. F.; Kubo, S. *Compos. Part A: Appl. Sci. Manuf.* **2004**, *35*, 395.
20. Compere, A. L.; Griffith, W. L.; Leitten, C. F.; Pickel, J. M. *Evaluation of Lignin from Alkaline-Pulped Hardwood Black Liquor* **2005**; Vol. *118*.
21. Srithep, Y.; Javadi, A.; Pilla, S.; Turng, L.; Gong, S.; Clemons, C.; Peng, J. *Polym. Eng. Sci.* **2011**, *51*, 1023.
22. Spinace, M. A. S. D.; Paoli, M. A. *J. Appl. Polym. Sci.* **2001**, *80*, 20.
23. Pesetskii, S. S.; Jurkowski, B.; Filimonov, O. V.; Koval, V. N.; Golubovich, V. V. *J. Appl. Polym. Sci.* **2010**, *119*, 225.
24. Chen, C.; Wang, L.; Huang, Y. *Chem. Eng. J.* **2009**, *150*, 269.
25. Hao, J.; Lei, G.; Li, Z.; Wu, L.; Xiao, Q.; Wang, L. *J. Membr. Sci.* **2013**, *428*, 11.
26. Hadjizadeh, A.; Ajji, A.; Bureau, M. N. *J. Mech. Behav. Biomed. Mater.* **2011**, *4*, 340.
27. Svinterikos, E.; Zuburtikudis, I. *Under Submiss.* **2016**,
28. Choi, D. I.; Lee, J. N.; Song, J.; Kang, P. H.; Park, J. K.; Lee, Y. M. *J. Solid State Electrochem.* **2013**, *17*, 2471.
29. Dallmeyer, I.; Ko, F.; Kadla, J. F. *Ind. Eng. Chem. Res.* **2014**, *53*, 2697.

30. Dallmeyer, I.; Ko, F.; Kadla, J. F. *J. Wood Chem. Technol.* **2010**, *30*, 315.
31. Morrison, I. M.; Stewart, D. *Phytochemistry* **1998**, *49*, 1555.
32. Dong, D.; Sun, J.; Huang, F.; Gao, Q.; Wang, Y.; Li, R. *Biomass Bioenergy* **2009**, *33*, 1719.
33. Poirier, N.; Derenne, S.; Balesdent, J.; Mariotti, a.; Massiot, D.; Largeau, C. *Eur. J. Soil Sci.* **2003**, *54*, 243.
34. Fanta, G. F.; Abbott, T. P.; Herman, A. I.; Burr, R. C.; Doane, W. M. *Biotechnol. Bioeng.* **1984**, *26*, 1122.
35. Rodrigues, B. V. M.; Ramires, E. C.; Santos, R. P. O.; Frollini, E. *J. Appl. Polym. Sci.* **2015**, *132*, DOI: 10.1002/app.41826.
36. Santos, R. P. O.; Rodrigues, B. V. M.; Ramires, E. C.; Ruvolo-Filho, A. C.; Frollini, E. *Ind. Crops Prod.* **2015**, *72*, 1.
37. Li, Y.; Huang, Z.; Lǔ, Y. *Eur. Polym. J.* **2006**, *42*, 1696.
38. Thompson, C. J.; Chase, G. G.; Yarin, A. L.; Reneker, D. H. *Polymer (Guildf)* **2007**, *48*, 6913.
39. Awal, A.; Sain, M.; Chowdhury, M. *Compos. Part B: Eng.* **2011**, *42*, 1220.
40. Park, J. Y.; Lee, I. H.; Bea, G. N. *J. Ind. Eng. Chem.* **2008**, *14*, 707.
41. Cramariuc, B.; Cramariuc, R.; Scarlet, R.; Manea, L. R.; Lupu, I. G.; Cramariuc, O. *J. Electrostat.* **2013**, *71*, 189.
42. Kong, L.; Ziegler, G. R. *Carbohydr. Polym.* **2013**, *92*, 1416.
43. Heikkilä, P.; Harlin, A. *Eur. Polym. J.* **2008**, *44*, 3067.
44. Montgomery, D. Design and Analysis of Experiments, 8th ed.; Wiley, **2013**; Chapter 11.
45. Minu, K.; Jiby, K. K.; Kishore, V. V. N. *Biomass Bioenergy* **2012**, *39*, 210.
46. Watanabe, H.; Shimomura, K.; Okazaki, K. *Proc. Combust. Inst.* **2013**, *34*, 2339.
47. Azadfar, M.; Gao, A. H.; Chen, S. *Int. J. Biol. Macromol.* **2015**, *75*, 58.
48. Alekhina, M.; Ershova, O.; Ebert, A.; Heikkinen, S.; Sixta, H. *Ind. Crops Prod.* **2015**, *66*, 220.
49. Sharma, R. K.; Wooten, J. B.; Baliga, V. L.; Lin, X.; Geoffrey Chan, W.; Hajaligol, M. R. *Fuel* **2004**, *83*, 1469.
50. Djebara, M.; Stoquert, J. P.; Abdesselam, M.; Muller, D.; Chami, A. C. *Nucl. Instruments Methods Phys. Res. B* **2012**, *274*, 70.
51. Mancera, A.; Fierro, V.; Pizzi, A.; Dumarçay, S.; Gérardin, P.; Velásquez, J. *Polym. Degrad. Stabil.* **2010**, *95*, 470.
52. García, A.; Toledano, A.; Serrano, L.; Egüés, I.; González, M.; Marín, F.; Labidi, J. *Sep. Purif. Technol.* **2009**, *68*, 193.
53. Andanson, J. M.; Kazarian, S. G. *Macromol. Symp.* **2008**, *265*, 195.
54. Wellen, R. M. R.; Canedo, E. L. *Polym. Test.* **2015**, *41*, 26.
55. Tejado, A.; Pen, C.; Labidi, J.; Echeverria, J. M.; Mondragon, I. *Bioresour. Technol.* **2007**, *98*, 1655.
56. Thakur, V. K.; Thakur, M. K.; Raghavan, P.; Kessler, M. R. *ACS Sustain. Chem. Eng.* **2014**, *2*, 1072.
57. Wang, S.; Li, Y.; Xiang, H.; Zhou, Z.; Chang, T.; Zhu, M. *Compos. Sci. Technol.* **2015**, *119*, 20.
58. Gordobil, O.; Egüés, I.; Llano-ponte, R.; Labidi, J. *Polym. Degrad. Stabil.* **2014**, *108*, 330.